

## Multiscale analysis of the geophysical lineaments of the High Plateaus (Eastern Morocco): structural implications

Jamila ABDERBI<sup>1,2\*</sup>, Driss KHATTACH<sup>1</sup>, Jamila KENAFI<sup>2</sup>

<sup>1</sup>Laboratory of Applied Geosciences and Center of Eastern Science and Water Technology, Department of Geology, Faculty of Sciences, Mohammed 1st University, Oujda, Morocco.

<sup>2</sup>Regional Center for the Professions of Education and Training (CRMEF), Oujda, Morocco.

Received 06 Apr 2016,  
Revised 27 Sep 2016,  
Accepted 03 Oct 2016

### Keywords

- ✓ Morocco,
- ✓ High Plateaus,
- ✓ aeromagnetic and gravity data,
- ✓ structural lineaments

### E-mail:

[jamila\\_abderbi@yahoo.fr](mailto:jamila_abderbi@yahoo.fr);

Tél: +212 536 50 48 50

### Abstract

The gravity and aeromagnetic data of High Plateaus (Eastern Morocco) have been reinterpreted by means of a multiscale analysis of the geophysical lineaments. These data were acquired as part of a national exploration project of mineral, groundwater, and hydrocarbon resources. The gravity and magnetic data were analyzed using the horizontal gradient coupled to the upward continuation and Euler deconvolution techniques to image the subsurface structures. These analyses show that the area is characterized by a prevalence of NE-SW lineaments. It includes possible old inherited tectonic structural features which may provide important controls on later basin architecture and evolution as well. Depth analysis indicates that the surface faults may extend to 5km depth. A new sketch map of structural elements was compiled from the aeromagnetic and gravity data interpretation over the High Plateaus area. It includes possible faults, folds and an inferred lithological boundary. This map constitutes a useful document for rationalizing the future research exploration in the area.

### 1. Introduction

The High Plateaus (HP) are located on the eastern Morocco, and are bounded by Jerada Mountains to the north, the eastern High Atlas belt to the south, the Algero-Moroccan frontier to the East and the termination of the Rekkam to the West. The Trarit divides this region into two areas: the Northern HP and Southern HP.

The HP lies roughly at 1200 to 1300 meters in elevation. They do not show any sign of disturbance compared to the northern and southern margins where the deformation is represented by folding and faulting. The area of study appears less tectonically affected because its architecture characters are sealed by the Plio-Quaternary sediments and outcrops of older rocks are poor.

During the years 1959, 1962 and 1963, the Moroccan Geological Survey and Mining Authority launched a project to acquire aeromagnetic and gravity surveys covering the entire HP. Magnetic and gravity data are commonly used to map the contacts between rocks that have different physical properties and such contacts commonly occur along fault boundaries. In petroleum or groundwater explorations, for example, magnetic and gravity anomalies often provides a good tool to study the old inherited subsurface structural features, which may provide important controls on later basin architecture and evolution as well.

In order to success such studies, the interpreter must have a good understanding of the structural and lithological framework and regional depositional patterns. In this study, a multiscale analysis of the geophysical data was used in order to delineate the lithological boundaries and subsurface faults [1-11]. The techniques employed were the horizontal derivative in coordination with the upward continuation and Euler deconvolution.

### 2. Geological and tectonic setting of the HP

The Figure 1 shows the geological map of the study area. Stratigraphically, the HP is a large and stable area with a sedimentary history ranging in age from the early Palaeozoic to Quaternary. The Palaeozoic sediments are formed by Carboniferous shale. The Mesozoic formations are characterized by Jurassic facies generally calcareous-dolomitica, while the formations of the Cretaceous are missing and are found only in the Southern HP. The Mio-Pliocene formations are characterized by a thick succession of more or less sandy clays, sands, sandstones and lacustrine limestone. The Quaternary deposits constitute the final stage of sedimentation; it is represented by calcareous crusts and conglomerate deposits [12].

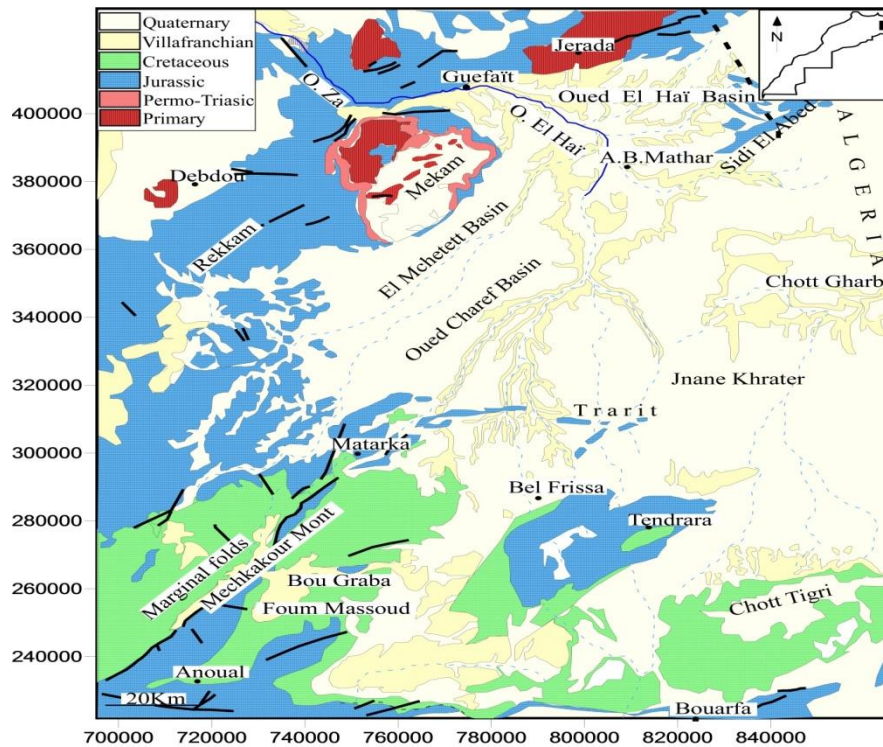


**Figure 1:** Simplified geological map and major structural elements of the Study area in High Plateaus.

Tectonically, the HP has been the seat of several geological studies that aimed to delineate the structural features of this area [12, 13].

The post Precambrian structural evolution of HP was marked by two major compressional events (Hercynian and Alpine orogenies) separated by an extensional period related to the Atlantic opening.

During the Hercynian orogeny, the east of Morocco was affected by polyphased deformation that reached its paroxysm at the Westphalian before it decreases gradually during the later phases. In HP, the earliest deformations of the Lower Palaeozoic and Devonian deposits are attributed to the Eovariscan phase, based on isotopic age dating of the metamorphic rocks. Metamorphism is important at Midelt and North Tamlelt whereas it is weak elsewhere. This tectono-metamorphic event has been dated at 366 Ma at Midelt and 370 Ma (Rb/Sr, [14]) and at Debdou-Mekkam (K/Ar on micas; [15]). The axes are oriented NNE–SSW, N–S, and NW–SE. Their vergence is generally towards the west [16, 17]. The late Hercynian deformations affect the Carboniferous rocks and overprint their substratum. They are folds and thrusts, NE–SW to E–W oriented. Their vergence is often to the north like at Jerada [18]. These deformations post-dated the Westphalian, as confirmed by isotopic ages at 300 Ma (K/Ar on micas; [15]). The granite emplacement ended afterwards, since the isotopic ages given by these authors are within the 286–247 Ma age interval [19].

During Alpine orogeny, the Mesozoic and Cenozoic geological evolution of HP can be viewed as a response to two major geological events:

The opening of the Atlantic and the Tethys in the early Mesozoic, High strain rates created by the thinning of the continental lithosphere resulted in the deformation of the crust by extension and rifting in the North African plate at the end of the Permian and the beginning of the Trias [20, 21]. In the Late Triassic–Early Cretaceous time (the synrift phase), NW–SE to NE–SW extensions occurred in the HP [22].

The peak of rifting occurring in the Jurassic was manifested by the opening of basins, under NW–SE, NE–SW to NS extension [22]. This Mesozoic extension involves the Variscan structures as normal faults [23].

The inversion of the rift systems took place at the Mesozoic–Cenozoic compressional–transpressional phases that controlled under the Africa–Europe continental collision [12, 21, 24–29].

The post Cretaceous deposits are represented by the marine formations and continental equivalent deposit, in relation to the Miocene transgression. The Messinian sediments uncomfortably cover all the structures.

The Cenozoic era came to an end with a continental or laguna sedimentation attributed to Quaternary age. The conglomerate, lacustrine limestone, loamy and stony continental deposit and particularly basalts of the Guercif area dated of 3.7–1.7 Ma, as well as basalts the ones of the Oujda area dated of 4.8–1.4 Ma [30] compose the main formations.

From the late Cretaceous to Quaternary, the HP records compressive events. The paroxysm of the deformation is manifested by the development of E–W folds associated with the vertical cleavage and faults in the northern part of this area [23]. The orientation of the higher stress component is WNW–ESE of Late Cretaceous–Paleocene, N–S of Eocene, NE–SW to NNE SSW for Early-Middle Tortonian and NW–SE of Plio-quaternary times [31,32, 33].

### 3. Material and methods

#### 3.1. Aeromagnetic and gravity data

During 1959, the HP area was covered by an aeromagnetic survey which was flown at a constant elevation of 1892 m above mean sea level. This campaign was performed along N-S flight lines whose mean spacing is 1.73 km (Fig.2). The magnetic variations and the international geomagnetic reference field (IGRF) were removed from the measured total magnetic field. The inclination and declination are  $-7.233^\circ$  and  $47.592^\circ$  respectively. The data were kindly provided by the Ministry of Energy and Mines. The corrected residual magnetic field data were gridded using the natural neighbor method with a grid spacing of 250 m. The residual aeromagnetic anomaly map obtained is show in Figure 3.

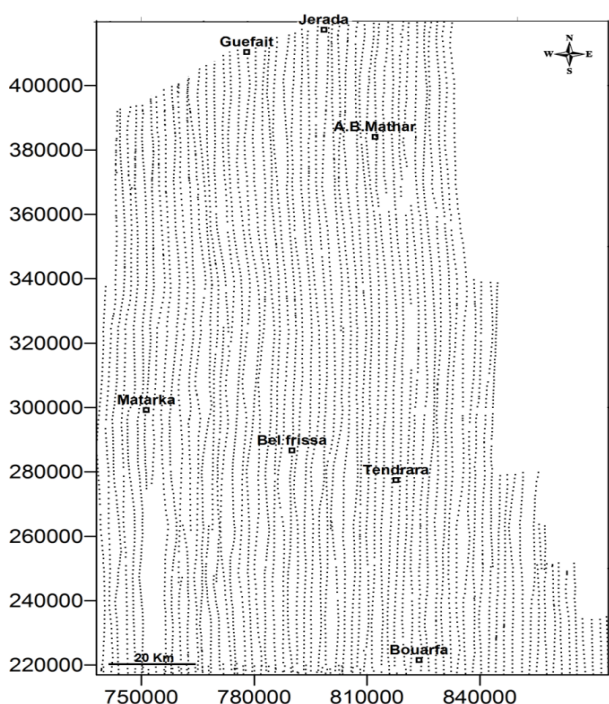


**Figure 2:** Location of the aeromagnetic data (Moroccan Lambert coordinates).

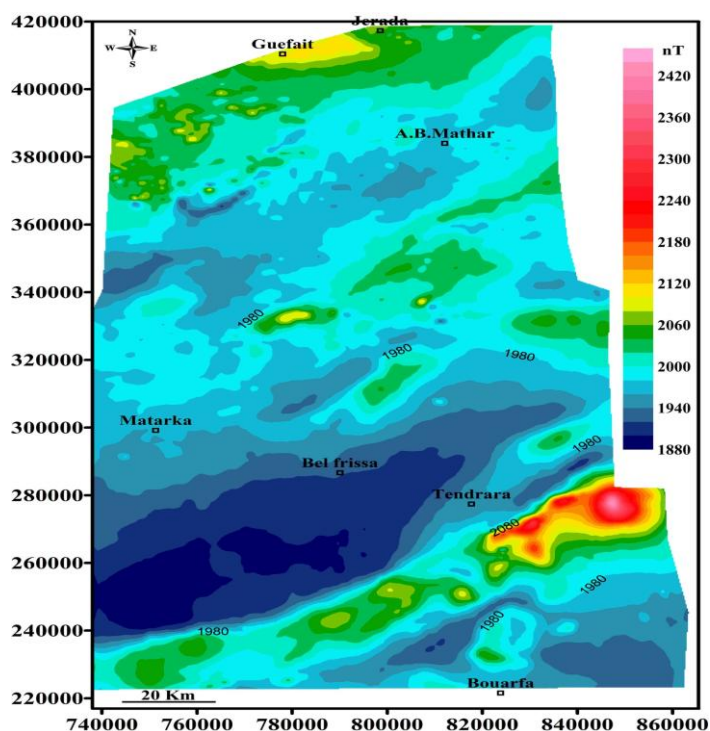


**Figure 3:** Residual aeromagnetic anomaly map of High Plateaus (Interval= 20 nT, Moroccan Lambert coordinates).

The interpretation of the magnetic anomalies is a complicated process because of the dipolar nature of magnetic field, the superposition of multiple magnetic sources and the presence of geological and cultural noises (pipe lines, power lines, railroads, and etc). Furthermore an observed anomaly has asymmetric shape, when magnetization occurs in anywhere rather than magnetic poles. This makes a dipolar nature on magnetic field which causes a horizontal displacement between measured anomaly and exact body location. The reduction to the pole (RTP) uses is an operator which transforms asymmetric anomaly to symmetric one by computing the effect of vertical. In frequency domain, according to [34], the RTP operator is:

$$A'(u,v) = \frac{A(u,v)}{(\sin I + i \cos I \sin(D + \alpha))^2}$$

where  $A(u,v)$ , is the amplitude at frequencies  $(u,v)$ ,  $I$  and  $D$  are the geomagnetic inclination and declination respectively and  $\alpha$  is  $\tan^{-1}(v/u)$ . The inclination and declination of the Earth magnetic field in the study area are respectively  $47.592^\circ$  and  $-7.233^\circ$ . Figure 4 shows the RTP magnetic anomaly map obtained of the study area

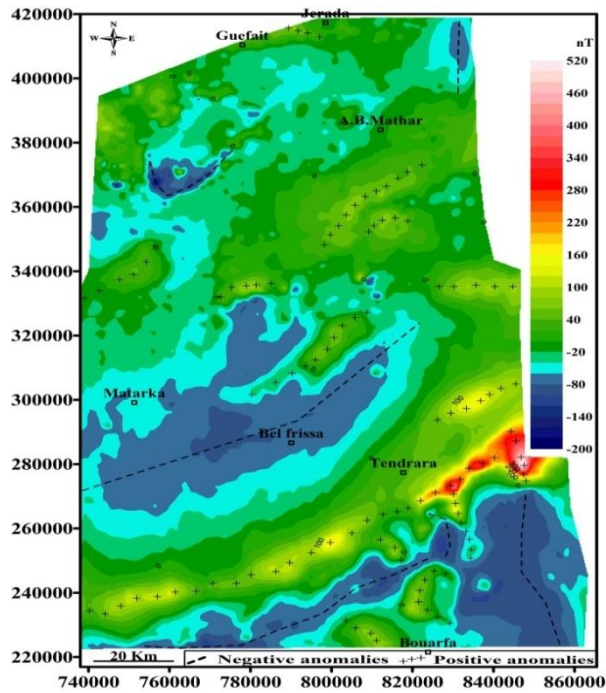


**Figure 4:** Residual aeromagnetic anomaly map reduced to north magnetic pole (Interval= 20 nT)

The gravity data of the HP area were recorded by the African Geophysical Company (A.G.C), during a regional survey performed in 1962 and 1963. These data are available as a Bouguer anomaly paper map established using a reduction density of  $2.5 \text{ g/cm}^3$ . This map was digitized, gridded with a mesh of 250 m and reproduced by contouring as it's shown on Figure 5. The residual gravity map in Figure 6 was calculated by eliminating the SW-NE regional effects induced by far-located bodies or by deep-seated sources. The used method is to calculate polynomial surfaces that adapt better to the data and subtract.

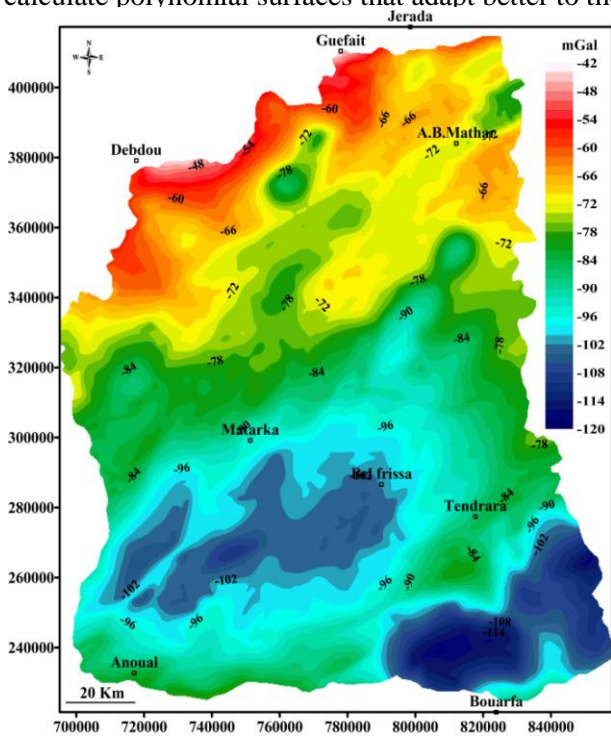


**Figure 5:** Bouguer anomaly Map of High Plateaus, (Interval= 2 mGal) Ministry of Energy and Mining, Rabat).

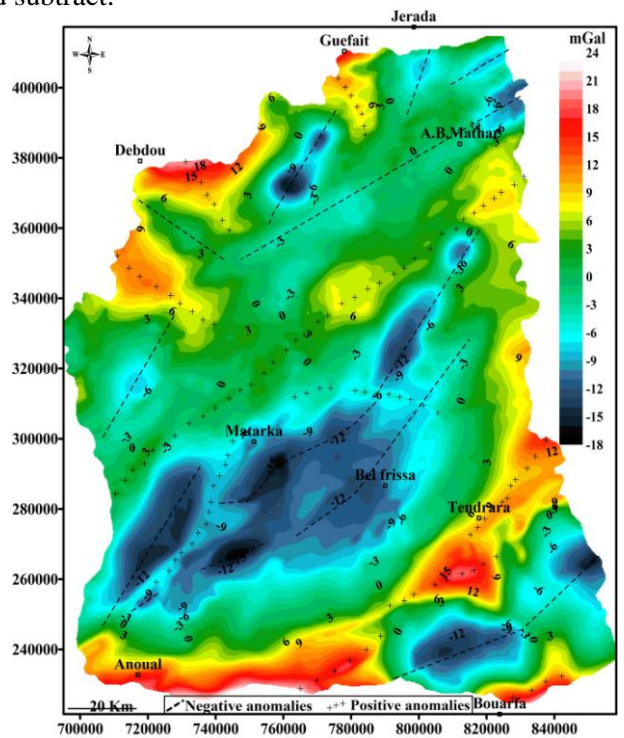


**Figure 6:** Residual Bouguer anomaly map of High Plateaus (Interval= 2 mGal, Moroccan Lambert coordinates).

### 3.2. Methodology

Two methods of analysis were employed for both gravity and aeromagnetic data in order to delineate lithological boundaries and faults:

\*Horizontal gradient (HG): This method has been used intensively to locate boundaries of density/magnetic contrast from potential field data. This method is also robust to delineation either shallow or deep sources in comparison with the vertical gradient, which is useful only for the shallower structures. Generally, sharp contacts evident in potential field data (gradients) are assumed to result from sharp discontinuities or interfaces between rock of contrasted properties (density or magnetic susceptibility) such as faults, unconformities or intrusive contacts. So, computing the horizontal gradients of the gravity and magnetic fields allow us to localize the limits of blocks and thus the fault position.

The horizontal gradient method, which involves mapping local maxima of the HG of gravity or pseudogravity [34], has been commonly used to locate the steepest parts of gradients associated with near-vertical physical-property boundaries, such as faults [1, 4, 35, ]. The amplitude of the horizontal gradient is expressed as:

$$GH = \sqrt{\left(\frac{\partial g}{\partial x}\right)^2 + \left(\frac{\partial g}{\partial y}\right)^2}$$

where  $(\partial g / \partial x)$  and  $(\partial g / \partial y)$  are the horizontal derivatives of the gravity field in the x and y directions.

A simple method for automated detection of these maxima is based on Blakely and Simpson's approach [1]. The procedure finds the location of maxima of a field defined on a regular grid by comparing the value at a central grid location in 3×3 grid window with that of its four pairs of surroundings grid points. A parabola is fitted through each of the four sets of the three points. A maximum of this parabola is accepted if it is located inside the central grid cell (square box around the central grid), and if its value exceeds that of the outer two points. In this case, several triplets reach a valid maximum, we used the location and value of the highest maximum. After obtaining the location of this maximum, several criteria can be applied to qualify it. Blakely and Simpson (1986) used the value of the maximum and an index N, which they defined as the number of valid maxima found in the 3×3 grid window. They found that indices 2 and 3 were most useful.

In order to determine the dip and the importance of faults, the horizontal gradient coupled to upward continuation method were applied to the gravity and magnetic data at several heights up to 4000 m by steps of 250 m. On each level the maximum of the horizontal gradient is localised. The overlay of horizontal derivative maxima at several heights underlines the various contacts and shows their dips. In the case of a dipping contact, the maxima move down dip with increasing continuation height. The linear contacts generally correspond to faults, whereas the contacts of circular form are the limits of intrusive bodies.

\*Euler deconvolution: This technique has been applied to both gravity and magnetic potential fields data. It provides fast information about the depth and the trends of the shallower subsurface structures in the area. The Euler deconvolution method can be traced back to [36] who first wrote down Euler's homogeneity equation for the magnetic case and derived the structural index that can be defined as a measure of the rate of change with distance of a field. Thompson [37] further studied and implemented the method by applying Euler deconvolution to synthetic and real magnetic data along profiles. Reid [38] followed up a suggestion by Thompson [37] and developed the equivalent method (3D Euler deconvolution), operating on gridded magnetic data. The 3D Euler's equation can be defined [38] as:

$$-N (T - B) = (x - x_0) \frac{\partial T}{\partial x} + (y - y_0) \frac{\partial T}{\partial y} + (z - z_0) \frac{\partial T}{\partial z}$$

where  $(x_0, y_0, z_0)$  are the coordinates of a magnetic source, the total-field T is measured at  $(x, y, z)$  and B is a base level, N indicates the structural index and relates to the geometry of the source. The structural index N defines the anomaly attenuation rate at the observation point and depends on the nature of the source; for example, N=0 for a simple contact, N=1 for the top of a vertical dike or the edge of a sill, N=2 for the center of a horizontal or vertical cylinder, and N=3 for the center of a magnetic sphere or a dipole [37, 38]. By considering four or more neighboring observations at a time (an operating window), source location  $(x_0, y_0, z_0)$  and B can be computed by solving a linear system of equations. Then by moving the operating window from one location to the next over the anomaly, multiple solutions for the same source are obtained [39]. Finally, a position where these solutions tend to cluster is considered to be the most likely location of the source.

### 4. Results and discussion

The reduction to the pole aeromagnetic anomaly map shows that the magnetic field of the study area is characterized by both low and high frequency anomalies with residual values ranging from 1800 to 2490 nT.

The low magnetic anomalies are associated with thick sedimentary cover which is mainly characterized by weak magnetic susceptibilities [11].

The Figure 6 shows the residual Bouguer anomaly map of the study area. The values are ranging from + 24 mGal. These variations are caused by rocks' density changes in subsurface related to lithological or structural contacts.

The detailed analysis of the HP's geophysical data shows a roughly good correlation between gravity and magnetic anomalies. From south to the north of the study area, the morphological similarities between the two anomalous fields clearly highlight linear subsurface sources having high magnetization and density. Nevertheless there is an apparent inverse correlation of some magnetic and gravity anomalies north of Bouarfa and Trarits; it indicates the presence of a granite intrusion in the region.

Generally, the positive anomalies are associated with an uplift or outcrop of the Palaeozoic basement and the negative anomalies indicating the presence of deep basins, salt domes or granites into basement. Most of the prevailing magnetic and gravity anomalies are trending in the NE-SW and ESE-WSW directions, suggesting that the causative structures are related to the main trend of the metamorphic Palaeozoic basement.

Horizontal gradient: The figures 7 and 8 present the contact analysis results for magnetic and gravity HP data. The maxima of the horizontal gradient computed for the residual maps of the two potential fields and for their upward continuations to different heights are overlain in order to the geological contacts and/or faults as well as their dip. These strong linear gradients materialize the brutal changes of magnetization and density within the basement.

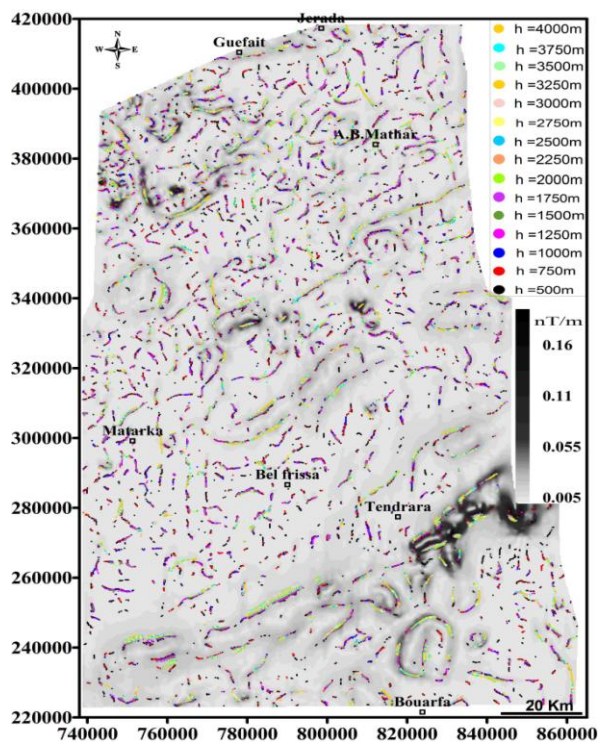


**Figure 7:** Horizontal gradient maxima of aeromagnetic anomaly map and its upward continuations to different heights (Moroccan Lambert coordinates).

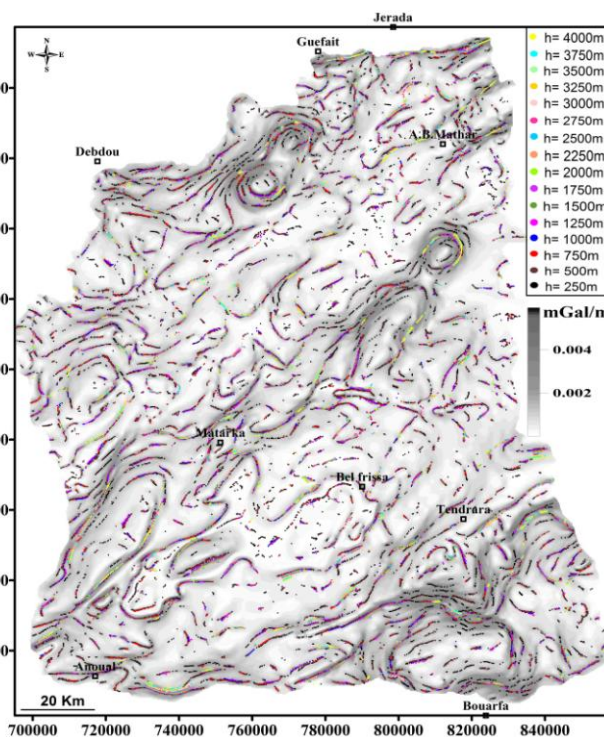


**Figure 8:** Horizontal gradient maxima of the residual Bouguer anomaly map and its upward continuations to different heights (Moroccan Lambert coordinates).

These lineaments interpreted as faults were traced out and statistically analyzed then represent as rose diagram (Fig. 9 and 10).

These lineaments could be divided into four families of directions. These are the N-S, NE-SW, ENE-WSW to E-W and NW-SE directions, with a clear prevalence of the NE-SW direction.

Euler deconvolution: The Euler solutions were computed using a window size of 10×10 data points to locate the possible subsurface structures and approximate depths of the aeromagnetic and gravity sources. For the aeromagnetic data a transformation must be applied to obtain depths with reference to the ground level. Thus a digital terrain model (DTM), provided by the Shuttle Radar Topography Mission (SRTM), was used.

The result of the Euler deconvolution of aeromagnetic and gravity data are depicted in Figures 11 and 12 respectively. This method permitted the identification of new subsurface faults as well as the mapping of known faults evident from the geological data. The interpretation of the Euler solutions indicated that the NE-SW and ENE-WSW to E-W trends primarily characterize the structural setting of the HP. The depths of these faults can reach 5960 and 2338 m for the magnetic and gravity lineaments respectively, we can thus advance that accident associated with these solutions would affect the basement and be inherited at least from Hercynian orogenies.

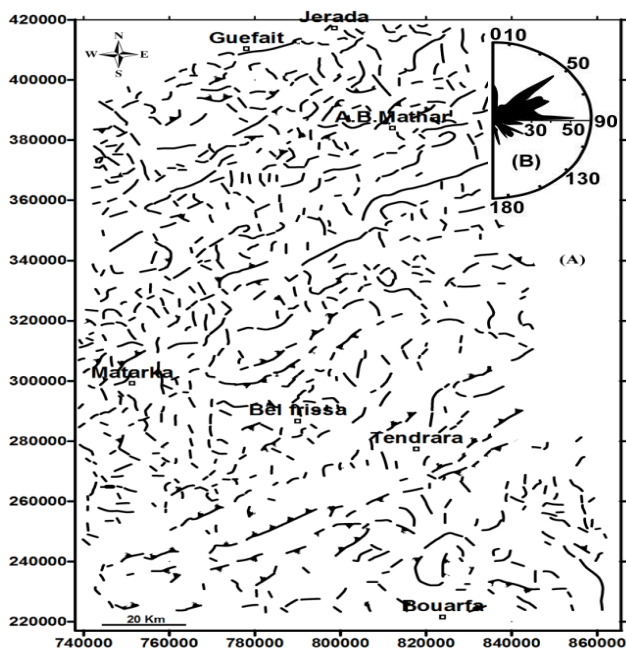


**Figure 9:** (A) Layout of the interpreted faults from the magnetic data (Moroccan Lambert coordinates), and (B) rose diagram frequencies.

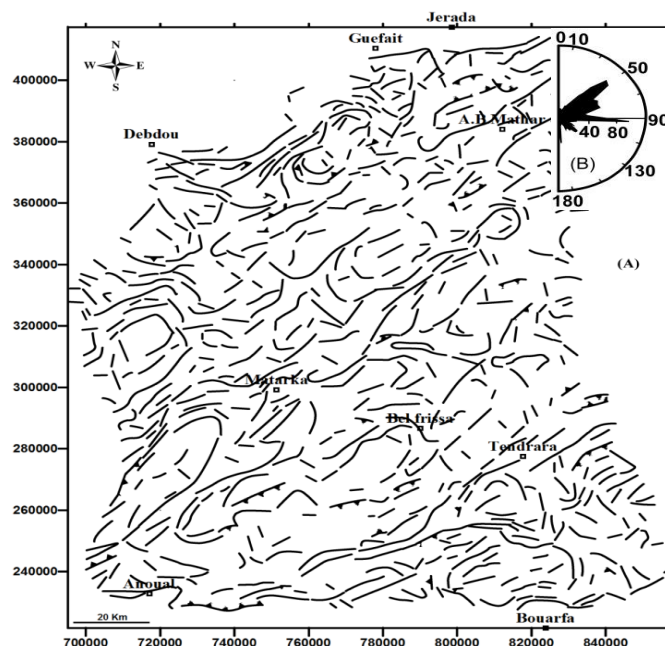


**Figure 10:** (A) Layout of the interpreted faults from the gravity data (Moroccan Lambert coordinates) and (B) rose diagram frequencies.

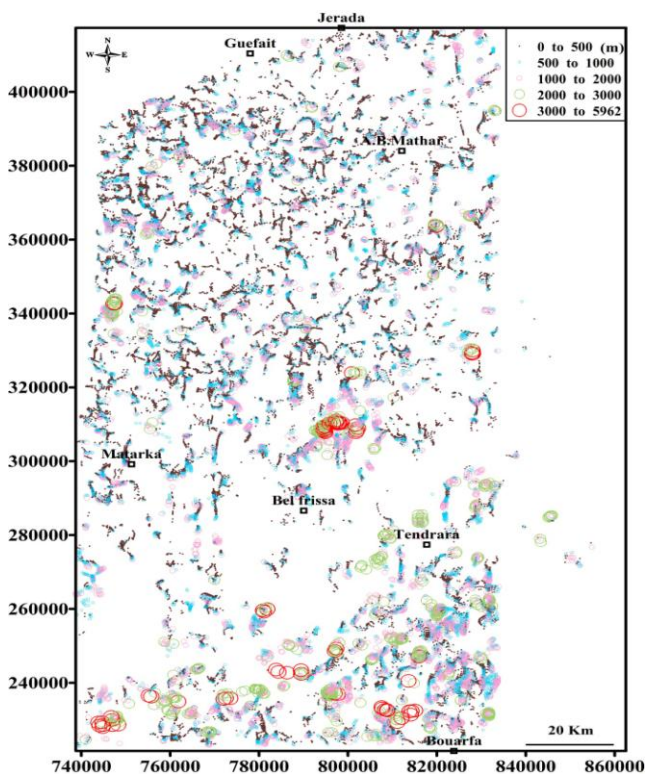


**Figure 11:** Euler deconvolution solution of the aeromagnetic anomaly in High Plateaus (IS= 0.5; window= 10×10; relative error= 15%, Moroccan Lambert coordinates).

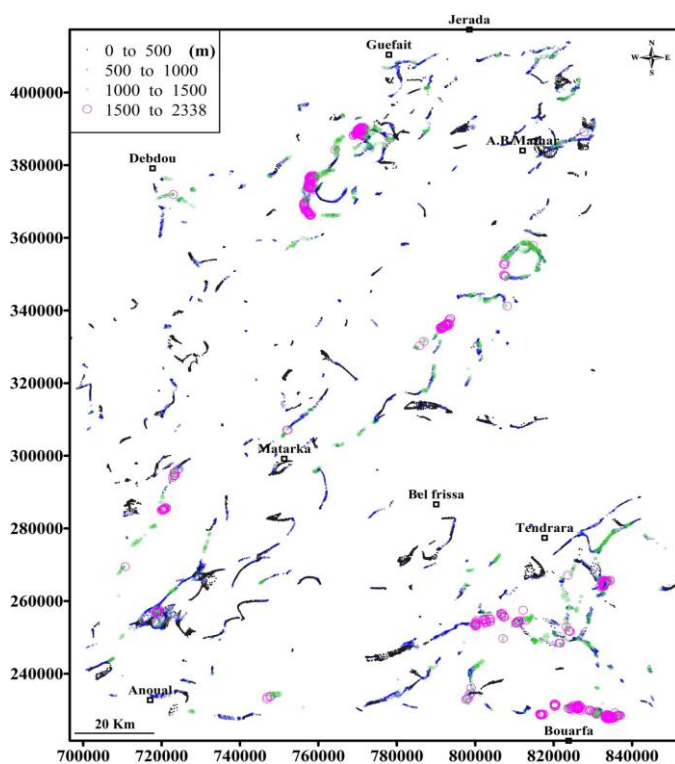


**Figure 12:** Euler deconvolution of Bouguer anomaly in High Plateaus (IS= 0.5; window= 10×10; relative error= 15%, Moroccan Lambert coordinates).

A statistical analysis was performed for the structural lineaments interpreted from both gravity and aeromagnetic data. After eliminating the repeated segments, a structural map of the HP area was (Fig. 13). This map shows the highlighted features are organized following four main directions: N-S, NE-SW, ENE-WSW to E-W and NW-WE.

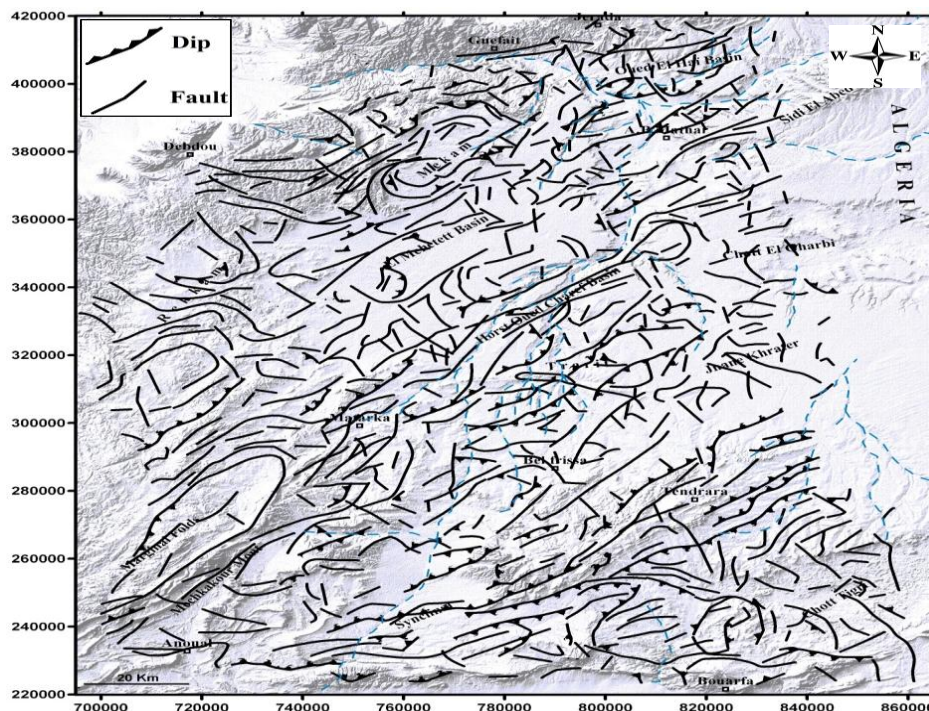


**Figure 13:** Interpreted tectonic map of High Plateaus, faults extracted from: the gravity and magnetic data (Moroccan Lambert coordinates).

The statistical results listed in Table 1, shows that a total number of 944 lineaments were identified with a cumulative length of 6048 km.

**Table 1:** Statistical analysis of the interpreted geophysical lineaments.

| Direction  | Frequencies | Frequencies % | total lengths | total lengths % |
|--|-------------|---------------|---------------|-----------------|
| N-S ( $0^{\circ}$ - $22,5^{\circ}$ / $157,5^{\circ}$ - $180^{\circ}$ ) | 166         | 16,86         | 707,19        | 11,69           |
| NE-SW ( $22,5^{\circ}$ - $67,5^{\circ}$ )                              | 375         | 38,11         | 2807,87       | 46,43           |
| ENE-WSW/ E-W ( $67,5^{\circ}$ - $112,5^{\circ}$ )                      | 240         | 24,39         | 1675,1        | 27,69           |
| NW-SE ( $112,5^{\circ}$ - $157,5^{\circ}$ )                            | 203         | 20,64         | 858,53        | 14,19           |
| Total  | 984         | 100           | 6048,42       | 100             |

These results indicate that the NE-SW lineaments predominate with a frequency of 38% and total length of 46%. They are followed by the ENE-WSW to E-W (24% frequencies, 28% total lengths). These main directions control the structural setting of HP. The other directions are less important, they include the NW-SE and N-S trends which have less significant frequencies and total lengths.

### Conclusion

The present study is devoted to shed more light on the structural settings of the HP area using interpretation of gravity and aeromagnetic data. The resulting structural map shows different subsurface bodies separated by major faults and/or contacts. According to these results, the following conclusions can be drawn:

- Four families of faults are distinguished trending in the NE-SW, ENE-WSW to E-W, NW-SE and N-S directions.
- The results confirm the existence of the faults that are already recognized such as Guefai and Anoual-Bouarfa Faults and specified their layout and dips. Some faults are not detected by the used techniques because of the weak density and/or magnetic susceptibility contrast or weak density of measurements.
- The synthetic structural map shows two major orientations: NE-SW and ENE-WSW to E-W. The two orientations, ENE-WSW to E-W (Tethyan) and NE-SW (Atlantic) have played a key role and reflect the structure of the High and Middle Atlas of Morocco.

- The NE–SW faults are parallel to the Hercynian belt in western Meseta of Morocco where the paroxysmal deformation occurred during Westphalian time while the ENE–WSW faults were later event in the Palaeozoic. It is suggested that the ENE–WSW to E–W lineaments are inherited from the Late E–W Carboniferous dextral transpression affecting the Atlas chain. The faults trending N–S affect shallow depths and remain superficial; it will be a recent character in relation with late Alpine compression events. The NW–SE direction is reactivated from the Palaeozoic to Quaternary. In this network NW–SE faults, there is an affinity between the eastern Meseta and Anti-Atlas by the faults or structures having N120 to N150 trend. The results will contribute to improve the structural map of the area and will be a very useful document in the planning of further hydrogeological or mining investigations.

**Acknowledgements**-The authors wish to thank the Ministry of Energy and Mining, Rabat, for providing aeromagnetic and gravity data used in this study.

## References

1. Blakely R.J., Simpson R.W., *Geophysics* 51 (1986) 1494.
2. Blakely R.J., *University of Cambridge* (1996) 461.
3. Cordell L., Grauch V.J.S., *Ann. Int. Meet. Soc. Explor. Geophys. Dallas* 52 (1982) 246.
4. Cordell L., Grauch V.J.S., *Soc. Explor. Geophys.* (1985) 181.
5. Everaerst M., Mansy J.L., *Bull. Soc. Géo. Fr.* 172 (2001) 267.
6. Vanié L.T.A., Khattach D., Houari M.R., *Bull. Ins. Sci. Rabat* 27 (2005) 29.
7. Khattach D., Mraoui H., Sbibih D., Chennouf T., *C. R. Geosci.* 338 (2006) 521.
8. Chennouf T., Khattach D., Milhi A., Andrieux P., Keating P., *C. R. Geosci.* 339 (2007) 383.
9. El Gout R., Khattach D., Houari M.R., Kaufmann O., Aqil H., *J. Afr. Earth. Sci.* 58 (2010) 255.
10. Abderbi J., Khattach D., *Bull. Ins. Sci. Rabat* 32 (2010) 19.
11. Abderbi J., Khattach D., *J. hydrocarb. mines environ. res.* 2 (2011) 111.
12. Medioni R., *Notes et Mém. Serv. Géol. Maroc* 41 (1970) 25.
13. Michard A., *Notes et Mém. Serv. Géol. Maroc* 252 (1976) 408.
14. Clauer N., Jeannette D., Tisserant D., *Geol. Rundsch.* 69 (1980) 63.
15. Huon S., Cornée J.J., Piqué A., Rais N., Clauer N., Liewig N., Zayane R., *Bull. Soc. Géo. Fr.* 164 (1987) 165.
16. Hoepffner Ch., *University of Strasbourg* 1 (1987) 280.
17. Houari M.R., Hoepffner C.h., *Afr. Geosci. Rev.* 7 (2000) 39.
18. Erraji A., *Faculté des Sciences de Rabat* (1997) 236.
19. Mrini Z., Rafi A., Duthou J.L., Vidal P.H., *Bull. Soc. Géo. Fr.* 281 (1992) 291.
20. Brede R., Hauptmann M., Herbig H., *Geol. Rundsch.* 81 (1992) 127.
21. Beauchamp W., Barazangi., Demnati A., El Alji A., *AAPG Bull.* 80 (1996) 1459.
22. Ait Brahim L., Chotin P., Hinaj S., Abdelouafi A., El Adraoui A., Nakcha C., Dhont D., Charroud M., Sossey Alaoui F., Amrhar M., Bouaza A., Tabyaoui H., Chaoui A., *Tectonophysics* 357 (2002) 187.
23. Hervouet Y., *Rev. Géogra. Phy. Géol. Dyn.* 27 (1986) 25.
24. Mattauer M., Taponnier P., Proust F., *Bull. Soc. Géo. Fr.* 7 (1977) 521.
25. Bensaid M., Kutina J., Mahmood A., Saadi M., *Glob. Tect. Metall.* 3 (1985) 59.
26. Piqué A., *Notes et Mém. Serv. Géol. Maroc* 321 (1987) 41.
27. Jacobshagen V., Brede R., Hauptmann M., Heinitz W., Zylka R., *Lect. Notes Earth Sci.* 15 (1988) 245.
28. Dewey J.F., Helman M.I., Turco E., Hutton D.H.W., Knott S.D., *Geo. Soc. London* 45 (1989) 265.
29. Westaway R., *Earth and Plan. Sci. Lett.* 96 (1990) 393.
30. Hernandez J., *University of Paris* 6 (1983) 418.
31. Ait Brahim L., *Faculté des Sciences de Rabat* (1991) 233.
32. Chotin P., Ait Brahim L., Tabyaoui H., *Mém. Muséum. Nat. hist. Natur. Paris* 182 (2000) 107.
33. Tabyaoui H., Ait Brahim L., Tahiri A., Chotin P., *Rev. Géol. Méditerran. Marseille* 3 (2000) 231.
34. Baranov V., *Geophysics* 22 (1957) 359.
35. Cordell L., *Geol Soc. Guidebook* 21 (1970) 158.
36. Hood P., *Geophysics* 30 (1965) 891.
37. Thompson D.T., *Geophysics* 47 (1982) 31.
38. Reid A.B., Allsop J.M., Granser H., Millett A.J., Somerton I.W., *Geophysics* 55 (1990) 80.
39. Ravat D., *J. Env. Eng. Geophysics* 1 (1996) 229.

(2017) ; <http://www.jmaterenvironsci.com>